



A new photocatalytic tool in VOCs abatement: Effective synergistic combination of sonication and light for the synthesis of monometallic palladium-containing TiO₂

Juan C. Colmenares ^{*}, Agnieszka Magdziarz ^{**}, Dariusz Łomot, Olga Chernyayeva, Dmytro Lisovytskiy

Institute of Physical Chemistry PAS, Kasprzaka 44/52, 01-224 Warsaw, Poland

ARTICLE INFO

Article history:

Received 1 August 2013

Received in revised form

17 September 2013

Accepted 19 September 2013

Available online 28 September 2013

Keywords:

TiO₂

Palladium

Sonophotodeposition

Methanol photo-oxidation

Sonication

ABSTRACT

A new simultaneous combination of ultrasonication and ultraviolet irradiation was proposed to synthesize materials with photocatalytic properties. Different palladium modified TiO₂ systems were synthesized, using commercial TiO₂ P90 as a support. Morphological and surface characterization of the samples as well as photocatalytic activity for methanol photo-oxidation was studied. Among different characterization techniques X-ray diffraction, diffuse reflectance UV-vis spectroscopy, N₂ physisorption, X-ray photoelectron spectroscopy, high resolution transmission electron microscopy with X-ray micro-analysis (HRTEM-EDS) were applied. Degradation of methanol was studied in the gas phase. The results of this study demonstrate that palladium in the reduced form was obtained in sonophotodeposition method (SPD), although the calcination step at 300 °C in air flow during 4 h was the last in the synthesis procedure. All Pd modified photocatalysts obtained by SPD method were very active (>90%) in gas phase methanol degradation and highly selective (>80%) to CO₂. The optimum palladium loading was fixed at 1 wt. %.

© 2013 Elsevier B.V. All rights reserved.

1. Introduction

The time that people spend inside buildings and closed areas is getting longer and longer and nowadays has risen up to 80% of their life [1]. This alarming number provoked some time ago an intensive scientific research for an efficient method to fight with indoor air pollution. In urban and industrial areas volatile organic compounds (VOCs) are the main sources of human health problems (e.g. headache, mucous membrane irritation, fatigue often recognized as SBS – sick building syndrome) [2,3]. Some of VOCs, e.g. benzene and its derivatives, haloalkanes, formaldehyde, amines etc., have been even detected as carcinogenic, mutagenic or teratogenic [4]. The list of VOCs sources is long and includes e.g. cooking and tobacco smoke, building materials, furnishings, dry cleaning agents, paints, glues, cosmetics, textiles, plastics, polishes, disinfectants, household insecticides, and combustion sources [5–7]. Obviously modern society cannot avoid them, therefore an effective method to eliminate VOCs from the air that people breathe is urgently needed.

Conventionally, indoor air pollution can be controlled by manipulating pollution sources, increasing the air exchange rate and using air purifiers [8]. Air purifiers, the most common among the above mentioned methods, employ filters to remove particulate matters or use sorption materials (e.g. granular activated carbon) to adsorb gases or odors. However, such techniques rather transfer the contaminants to another phase than eliminate them and additionally are not cost effective [9]. The future of efficient air purification lies in advanced oxidation processes (AOPs) in which pollutants are completely oxidized to CO₂ and H₂O. According to many researchers photocatalytic oxidation (PCO) is one of the most promising technologies among oxidation processes [10–15]. There are several advantages that make it more attractive than other oxidative methods: (1) ambient temperature and pressure, (2) inexpensive catalyst material, (3) mild oxidation conditions, (4) oxidative potential toward various contaminants [16].

Invariably a good photocatalyst is described as photoactive, able to utilize visible and/or near UV light, biologically and chemically inert, photostable, inexpensive and non-toxic [7]. Among the group of metal oxides or sulfides, e.g. TiO₂, ZnO, ZrO₂, SnO₂, WO₃, CeO₂, Fe₂O₃, Al₂O₃, ZnS, CdS, that present semiconducting properties, still TiO₂ is the best choice for the majority of researchers [17]. However, more active and stable TiO₂ based photocatalyst is still in demand. One of the ways to make TiO₂ more active is to deposit some

* Corresponding author: Tel.: +48 223433215.

** Co-corresponding author: Tel.: +48 22 343 3360.

E-mail addresses: jcarloscolmenares@ichf.edu.pl (J.C. Colmenares), amagdziarz@ichf.edu.pl (A. Magdziarz).

noble metals (e.g. Pt or Pd) on the TiO₂ surface. Such deposition enhances the photocatalytic efficiency, because the metal can act as an electron trap, can promote interfacial charge transfer and finally can delay recombination of the electron–hole pair [18]. There are many reports that confirm the significant enhancement in activity after deposition of noble metals on the TiO₂ surface [19–22]. Herein, an economical issue is also important. Among the group of noble metals, which are generally expensive, there is an increasing interest in using palladium as metallization source. Firstly, is much cheaper than platinum and secondly, is 50 times more abundant on earth [23].

Sonication is currently considered one of the most powerful tools in the synthesis of nanomaterials. In comparison with traditional sources of energy, ultrasounds ensure unusual reaction conditions in liquid phase reactions due to the cavitation phenomenon (extremely high temperatures and pressures are formed in very short times in liquids) [24]. Chemical effect of ultrasound operation in liquids is the formation of free radicals, e.g. •H and •OH. Then, they can recombine to H₂O or interact to form H₂, H₂O₂ or •HO₂. These radicals and compounds, with strong oxidative and reductive properties, are sources of various sonochemical processes in aqueous solutions. Sonochemical reduction of noble metal salts has advantages over the other traditional reduction methods, because it does not require reducing agent, the reaction rates are reasonably fast and nanometric sized particles are produced [25]. Therefore, sonication is very often coupled with traditional synthesis methods, like sol-gel, photodeposition or wet impregnation [26–28].

Photodeposition process involves the reduction of aqueous metal ions by photo-induced electrons when they are excited from the valence band to the conduction band of semiconductor upon light irradiation. As a result, metallic particles are deposited on the surface of the semiconductor [29]. Although this method is easy to realize there are many reports that found it rather ineffective for obtaining noble metals over TiO₂ with high photocatalytic activity [30].

However, such photodeposition as well as sonication are often reported in the literature to be used in the synthesis of nanomaterials. Even so, these methods are usually applied individually or in the sequential combination, first sonication and later on photodeposition, what makes the whole process long [31,32]. Additionally, the use of reducing agents is also necessary. Therefore, a tentative idea has appeared to combine in situ ultrasonication with photocatalytic reduction of metal into so called sonophotodeposition method [33]. Herein, reducing agents are electrons produced as a result of the ultraviolet absorption by semiconducting material, while ultrasounds assure enhanced mass transfer between reagents and help in the metal reduction. Thus, the aim of this study was to synthesize palladium containing TiO₂ catalyst by a novel sonophotodeposition method and to investigate its catalytic behavior in a gas phase photocatalytic oxidation of a common organic pollutant such as methanol.

2. Experimental

2.1. Photocatalysts preparation

Palladium containing TiO₂ photocatalysts were prepared by a novel sonophotodeposition method [33]. Commercial TiO₂ (AEROXIDE TiO₂ P90, Evonik Industries) was used as a support. For this, 0.1 g of oxalic acid and desired amount of palladium (II) acetylacetone were dissolved in 120 mL H₂O:CH₃CN (30:70, v/v) and 0.5 g of TiO₂ was dispersed into this solution. The photocatalytic reactor with such prepared mixture was placed into the ultrasonic bath (35 kHz, 560 W, Sonorex Digitec-RC, Bandelin). The synthesis reaction was carried out under argon flow (flow rate 70 mL min⁻¹)

and at 20 °C. The suspension was first kept in the dark for 30 min to reach complete adsorption equilibrium. Sonophotodeposition was performed by illuminating the suspension for 60 min with a low pressure mercury lamp (6 W, λ_{max} = 254 nm) and with ultrasonic bath switched on. In Fig. 1 the synthesis reaction setup is presented. Then the product was recovered by slowly evaporation in rotary evaporator, dried at 110 °C for 10 h, and calcined at 300 °C for 4 h under air flow (flow rate 30 mL min⁻¹). The resulting photocatalysts were denoted as XPd/P90/SPD, where X stands for wt% of deposited palladium (in this study: 0.5, 1 and 2 wt%) and SPD for sonophotodeposition. For comparative purposes, a bare TiO₂ was treated by sonophotodeposition (denoted as P90/SPD) and conventional photodeposition method was used for the synthesis of 1%Pd/P90/PD.

2.2. Characterization methods

UV-vis diffuse reflectance spectra were recorded on a UV/VIS/NIR spectrophotometer Jasco V-570 equipped with an integrating sphere. The baseline was recorded using Spectralon™ (poly(tetrafluoroethylene)) as a reference material. To determine the band gap of the powders (E_g), the Kubelka–Munk method based on the diffuse reflectance spectra was employed. The E_g of the powders was calculated from the (f(R)hv)^{1/2} vs. hv plots. The function f(R) was calculated from the equation [34]: f(R) = (1-R)²/2R.

Powder XRD measurements were performed using standard Bragg–Brentano configuration. This type of arrangement was provided using Siemens D5000 diffractometer (equipped with a horizontal goniometer) with θ–2θ geometry and Ni filtered Cu Kα radiation, powered at 40 kV and 40 mA. Data were collected in the range of 2θ = 10°–90° (some data up to 120°) with step interval of 0.02° and counting time up to 5 s per step. The phase content of anatase over rutile was estimated from the respective XRD peak intensities using the following equation [35]: f_A = 1/[1+1.26(I_R/I_A)], where f_A is the fraction of anatase phase in the powder, and I_A, I_R are the diffraction intensities of the anatase (1 0 1) and rutile (1 1 0) crystalline phases at 2θ = 25.3 and 27.4°, respectively.

TEM and STEM studies were carried out using FEI TITAN Cubed electron microscope operated at an acceleration voltage of 300 keV and equipped with an energy dispersive X-ray (EDS) EDAX spectrometer. The samples were prepared by dispersing in pure alcohol using ultrasonic cleaner and putting a drop of this suspension on carbon films on copper grids and purified with plasma cleaner.

The XPS measurements were performed using a VG Scientific photoelectron spectrometer ESCALAB-210 using Al Kα radiation (1486.6 eV) from an X-ray source operating at 15 kV and 20 mA. Survey spectra were recorded for all the samples in the energy range from 0 to 1350 eV with 0.4 eV step. High resolution spectra were recorded with 0.1 eV step, 100 ms dwell time and 25 eV pass energy. Ninety degrees take-off angle was used in all measurements. The curve fitting was performed using the AVANTAGE software provided by Thermo Electron, which describes each component of the complex envelope as a Gaussian–Lorentzian sum function; a constant 0.3(±0.05) G/L ratio was used. The background was fitted using nonlinear Shirley model. Scofield sensitivity factors and measured transmission function were used for quantification. Aromatic carbon C 1s peak at 284.5 eV was used as reference of binding energy.

The specific surface area, pore volume, and average pore diameter were determined by N₂ physisorption using a Micromeritics ASAP 2020 automated system and the Brunauer–Emmet–Teller (BET) and the Barret–Joyner–Halenda (BJH) methods. Each sample was degassed under vacuum at <1 × 10⁻⁵ bar in the Micromeritics system at 300 °C for 4 h prior to N₂ physisorption.

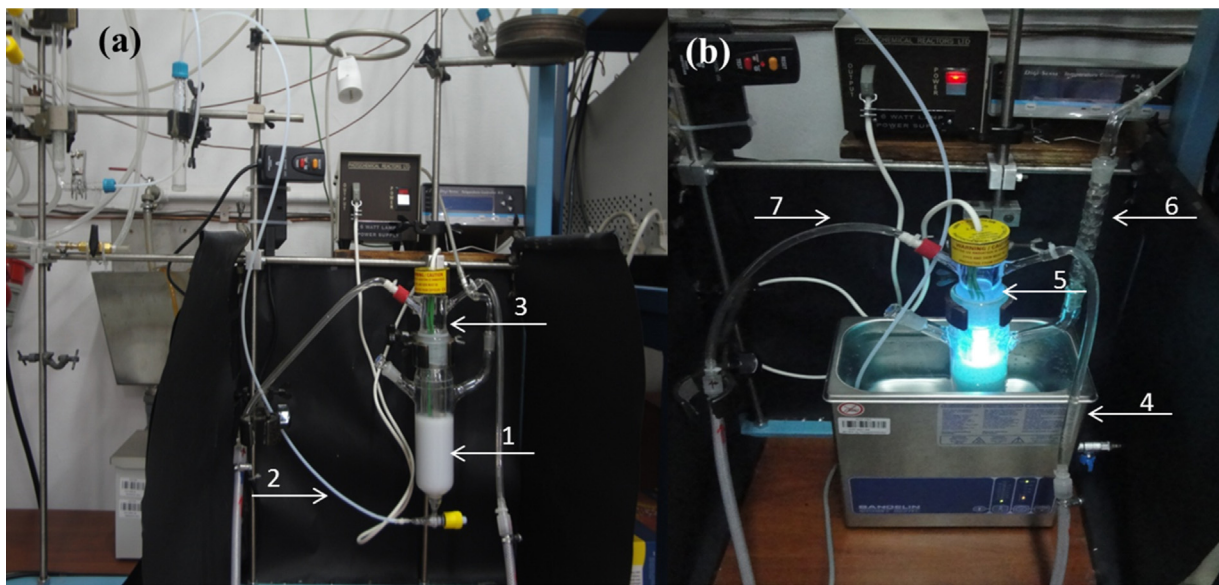


Fig. 1. Sonophotodeposition reaction setup before (a) and during the reaction (b):(1) batch reactor, (2) argon line, (3) switched off 6W UV lamp (4) ultrasonic bath (5) switched on 6W UV lamp, (6) reflux condenser, (7) lamp cooling system.

2.3. Photocatalytic activity measurements

All experiments of methanol photooxidation were carried out using a quartz micro-reactor connected to a quadrupole mass spectrometer (Dycor-Ametek MA200, USA) via a heated capillary and Balzers high-pressure gas inlet system. The adsorption equilibrium reagent–photocatalyst was achieved in the dark after 2 h in the flowing air ($25 \text{ cm}^3 \text{ min}^{-1}$) saturated with methanol at 0°C . A light source was a medium pressure 125 W mercury lamp ($\lambda_{\text{max}} = 365 \text{ nm}$; supplied by Photochemical Reactors Ltd. Model RQ 3010) placed inside the quartz immersion well and thermo stated at 30°C . The temperature was measured and was established at ca. 75°C during the whole reaction time (180 min). The setup scheme is presented in Fig. 2 [36]. In order to determine the changes in the relative amounts of various released gaseous species specified mass signals were chosen, so that the obtained signals were elaborated in terms of standard mass spectra of the respective compounds.

3. Results and discussion

3.1. Physico-chemical properties of the photocatalysts

Crystalline phase composition of the samples was studied by XRD. Fig. 3 shows the XRD patterns of photocatalysts prepared by sonophotodeposition (SPD) method with increasing palladium

content from 0 to 2 wt.%. For comparison a pattern of 1 wt.% of palladium deposited on TiO_2 P90 by photodeposition method and a pattern of commercial Evonik bare TiO_2 P90 samples were added. It is clearly seen that all photocatalysts consist of the mixture of anatase and rutile crystallite phase show ever the addition of palladium provoked few changes in the phase composition of TiO_2 . Titanium phase composition and crystallite sizes estimated by the Scherrer equation are listed in Table 1. In all palladium containing samples, prepared by sonophotodeposition method, the percentage of anatase crystallite phase is lower and the percentage of rutile crystallite phase is higher compared to both bare TiO_2 samples and 1 wt.%Pd/P90/PD. This difference increases with the higher loading of palladium giving almost double amount of rutile phase in the case of the highest Pd loading of 2 wt.% (85% of anatase and 15% of rutile for TiO_2 P90 and 71% of anatase and 29% for 2 wt.%Pd/P90/SPD). At the same time the crystallite sizes of anatase and rutile remained unchanged. In all palladium containing series some small peaks associated with the metal deposits were observable. The reflections were recorded at diffraction angles of $2\theta \sim 40^\circ$, $2\theta \sim 47^\circ$, $2\theta \sim 68^\circ$, $2\theta \sim 82^\circ$, $2\theta \sim 87^\circ$ corresponding to the (1 1 1), (2 0 0), (2 2 0), (3 1 1) and (2 2 2) planes of Pd^0 , respectively [37]. Additionally, in 1 wt.%Pd/P90/Photo sample another peak, characteristic for PdO crystallite phase ($2\theta \sim 34^\circ$) was recorded. It suggests coexistence of two crystallite phases (PdO and metallic Pd) in the photocatalyst prepared by photodeposition method, whereas sonophotodeposition method gives metal in its reduced form. Herein, a fully metallized form of palladium is obtained due to the combination of sonication with light. The crystallite sizes of palladium for the photocatalysts prepared by sonophotodeposition method are closed to each other (approx. 24 nm, Table 1).

In order to gain more information about the surface composition of the photocatalysts all samples were studied by XPS. The binding energies, oxidation states and atomic concentrations of Ti 2p, O 1s and Pd 3d of all palladium containing systems as well as bare TiO_2 (P90/SPD) are given in Table 2. In all samples the dominant peak of Ti 2p is located at $458.70 \pm 0.2 \text{ eV}$ and clearly corresponds to Ti^{4+} in TiO_2 structure [38]. Besides, in each sample ca. 10% of Ti^{2+} at the surface was also detected. In all palladium containing samples, synthesized by SPD method, only metallic Pd was identified at the surface by a peak located at $334.55 \pm 0.32 \text{ eV}$, although calcination in air was the last synthesis step. In contrast, in Pd- TiO_2 prepared

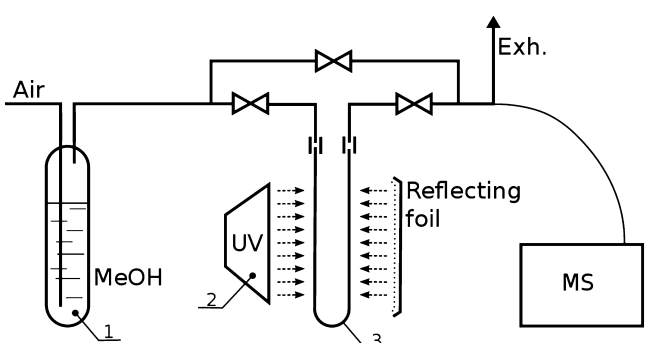


Fig. 2. Scheme of the reaction setup used in this study: (1) methanol, (2) 125 W UV lamp thermostated at 30°C , (3) reactor with photocatalyst [36].

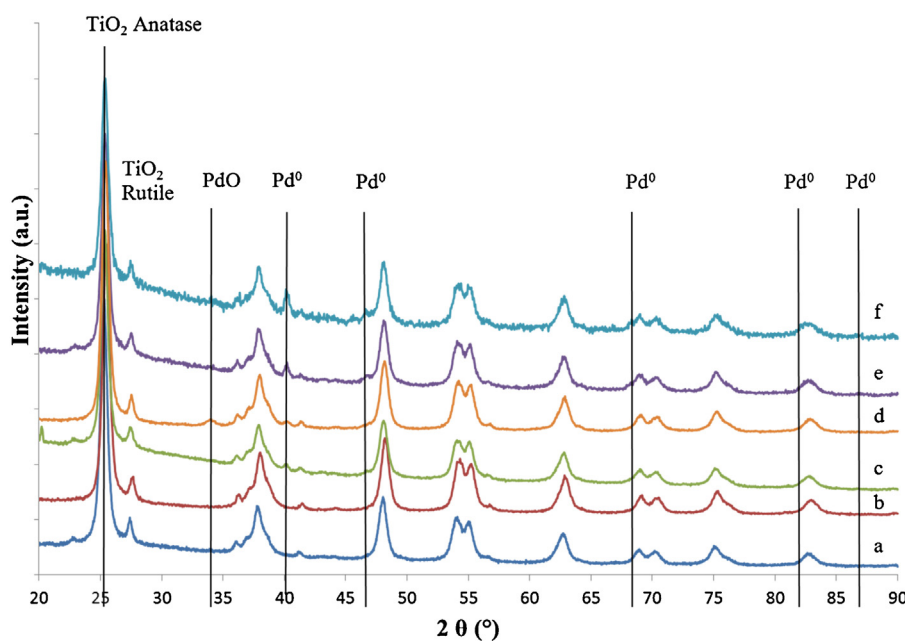


Fig. 3. XRD patterns of different photocatalysts: (a) P90, (b) P90/SPD, (c) 0.5%Pd/P90SPD, (d) 1%Pd/P90PD, (e) 1%Pd/P90SPD, (f) 2%Pd/P90SPD.

Table 1

Textural, structural and optical properties of palladium containing and bare TiO_2 photocatalysts (SPD stands for sonophotodeposition and PD stands for photodeposition method).

Photocatalyst	XRD Fraction (%) / diameter of TiO_2 (nm) ^a	Diameter of Pd (nm)	UV-vis Band gap (eV)	Absorption threshold (nm)	N_2 physisorption S_{BET} ($\text{m}^2 \text{g}^{-1}$) ^b	V_p ($\text{cm}^3 \text{g}^{-1}$) ^b	d_p BJH (nm) ^b
P90	A (85)/(12): R (15)/(23)	–	2.96	418	107	0.42	13.3
P90/SPD	A (84)/(12): R (16)/(22)	–	2.96	418	103	0.42	14.1
0.5%Pd/P90/SPD	A (73)/(12): R (27)/(23)	Pd ⁰ (24)	2.54	488	96	0.38	13.9
1%Pd/P90/SPD	A (74)/(12): R (26)/(26)	Pd ⁰ (24)	2.51	493	98	0.42	15.0
2%Pd/P90/SPD	A (71)/(12): R (29)/(27)	Pd ⁰ (24)	2.08	595	100	0.40	14.2
1%Pd/P90/PD	A (84)/(11): R (16)/(22)	Pd ⁰ (18):PdO (10)	2.43	509	104	0.41	13.7

^a A stands for anatase and R for rutile.

^b BET surface area (S_{BET}) calculated by Brunauer–Emmet–Teller (BJH) formula, cumulative pore volume (V_p), median pore width (d_p BJH) calculated by Barret–Joyner–Halenda (BJH) formula.

by photodeposition, Pd^{2+} ions in the form of PdO were found after calcination, according to the signal 336.29 eV [39]. XPS results are in a good agreement with XRD and confirm the hypothesis that the conditions applied in SPD method lead to obtain totally reduced metal nanoparticles, although the last step in the synthesis procedure is calcination in air flow (at 300 °C). Concerning low surface values of atomic ratios Pd/Ti , in comparison with the nominal values, it can be deduced that the main amount of deposited metal is located in the bulk of the material, not at the surface. However, it is enough to see high photocatalytic activity and selectivity.

Looking for more evidences regarding the nature of deposited palladium particles TEM measurements were employed. Selected micrographs of Pd/TiO_2 samples are shown in Fig. 4. The

micrograph of each sample consists of TEM image with a corresponding EDS spectrum and a graph presenting palladium particles distribution (inset). In all cases EDS analysis confirmed a successful deposition of palladium particles on the TiO_2 surface applying SPD method. As it can be observed in Fig. 4 in each system palladium particles mostly form spherically shaped agglomerations with a diameter from dozen to ca. 100 nm. The formation of these aggregates could be ascribed to the preparation technique of samples for TEM measurements. Concerning an average particle size of TiO_2 P90, ca. 12 nm basing on XRD measurements, the tendency to form aggregates is natural. Therefore the $\text{Pd}-\text{TiO}_2$ particles could agglomerate while waiting for alcohol evaporation before TEM analysis. Analyzing palladium particles distribution for each sample it results

Table 2

XPS results for all palladium modified TiO_2 and bare TiO_2 /SPD (SPD stands for sonophotodeposition and PD stands for photodeposition method).

Photocatalyst	Ti 2p _{3/2} BE eV (%) ^a		Pd 3d _{5/2} BE eV (%) ^a		O 1s BE eV (%) ^a		Pd/Ti atomic ratio		
	Ti ⁴⁺	Ti ²⁺	Pd ⁰	Pd ²⁺	Ti–O	O–Ti–O (Pd–O) ^b	O–C–O	Nominal	XPS
P90/SPD	458.78(90)	456.15 (10)	–	–	527.45(12)	529.83(58)	530.94(30)	–	–
0.5%Pd/P90/SPD	458.93(93)	455.93 (7)	334.55(100)	–	527.27(8)	530.14(78)	531.33(14)	0.005	0.0015
1%Pd/P90/SPD	458.70(92)	455.70 (8)	334.87(100)	–	526.96(6)	530.03(87)	531.65 (7)	0.01	0.0024
2%Pd/P90/SPD	458.70(92)	455.68 (8)	334.73(100)	–	527.16(7)	530.03(77)	531.19 (16)	0.02	0.0033
1%Pd/P90/PD	458.87(90)	456.33 (10)	–	336.29 (100)	527.63(11)	529.63 (30)	530.7(59)	0.01	0.0033

^a Relative proportions in parentheses.

^b Only in the 1%Pd/P90/PD.

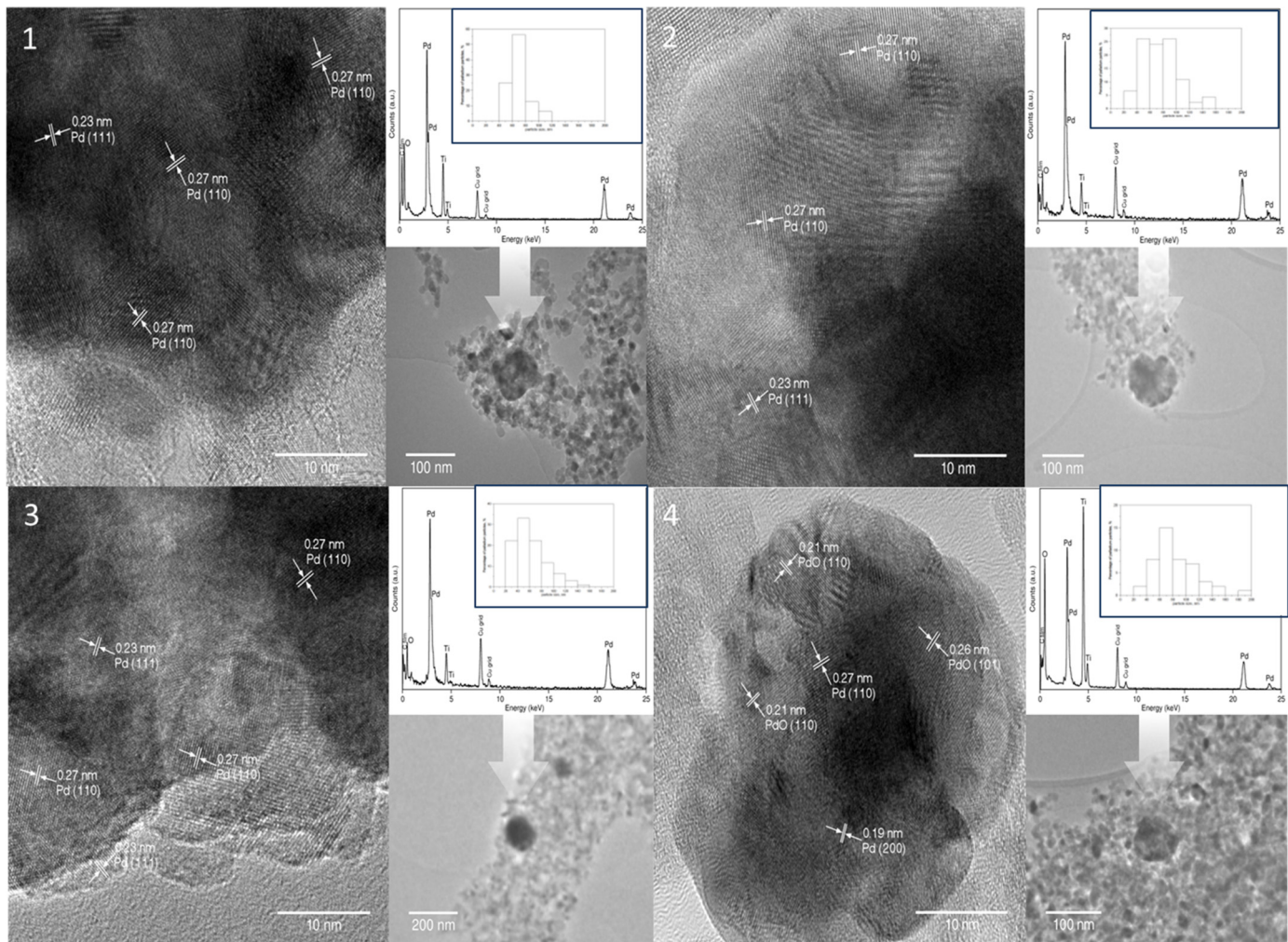


Fig. 4. TEM images with corresponding EDS spectra of the following samples: (1) and (1a) 0.5%Pd/P90SPD, (2) and (2a) 1%Pd/P90SPD, (3) and (3a) 2%Pd/P90SPD, (4) and (4a) 1%Pd/P90PD. Insets: palladium particles distribution (%) in terms of particle size (nm).

that using PD method only 10% of Pd particles in 1%Pd/P90/PD are below the size of 50 nm, whereas in the samples synthesized by SPD method it is 25%, 30% and 50% for 0.5%Pd/P90/SPD, 1%Pd/P90/SPD and 2%Pd/P90/SPD, respectively. Calculation of the separation between lattice fringes in Pd particles permits to define the crystallite phase of palladium. In Fig. 4(4), which presents the image of 1%Pd/P90/PD, both Pd^0 and PdO crystallite phases are recognized, whereas in the images of the photocatalysts prepared by SPD method (Fig. 4(1)–(3)) only metallic form of Pd is seen. These results are in a good complement of the previous discussed XRD and XPS techniques. Comparing TEM and XRD measurements it can be deduced that the aggregates seen on TEM images are built of crystallites of palladium nanoparticles with the approx. size of 24 nm measured by XRD (see Table 1). Additionally, the size of palladium agglomerates probably enabled detection of Pd^0 in the corresponding XRD, even for the lowest metal loading.

The shape of a gas adsorption isotherm is a source of qualitative structural information of the material. Adsorption on mesoporous solids proceeds via multilayer adsorption followed by capillary condensation and its graphical representation are type IV and V isotherms [40]. Mesoporosity of the photocatalysts was confirmed by N_2 adsorption–desorption measurements. All of the samples, with and without Pd modification, showed type IV isotherms with H1 hysteresis loop and the corresponding narrow pore size distribution curves (results not shown here) that are typical of

mesoporous materials with well-defined uniform mesopores [41]. The physicochemical properties of these samples are listed in Table 1. Regarding the specific surface area values (Table 1) it was found that Pd modification, by both methods SPD and PD, did not appreciably affect the surface area of the TiO_2 and the pore volume. It suggests that palladium was mostly deposited on the surface of the support [42] and not inside the pores of TiO_2 . This observation correlates well with the XRD results, as the crystallite Pd sizes (up to 26 nm) are too big to enter into the pores (average ca. 14 nm).

Light absorption properties of the samples were studied by UV–vis spectroscopy. Fig. 5 depicts diffuse reflection spectra of all, palladium containing and bare, samples. The bare TiO_2 samples are white, while all Pd modified TiO_2 are gray, thus indicating a change in their optical properties [23]. It is seen that the absorbance in the visible region is higher for all Pd containing samples than for bare TiO_2 . A broad band between 450 and 550 nm centred at 470 nm was observed in the absorption spectra of 1%Pd/P90/PD, owing to a d–d transition of PdO particles [43]. This is evidence, supplementary to the techniques discussed above, of PdO crystallite form obtained by photodeposition method. Obviously, this band was not observed in the spectrum of all photocatalysts made by SPD method. All calculated band gap values (correlation coefficient $R^2 > 0.99$) are summarized in Table 1. A significant red shift in the visible region is observed for all Pd containing samples, especially for 2%Pd/P90/SPD photocatalyst ($E_g = 2.08$ eV).

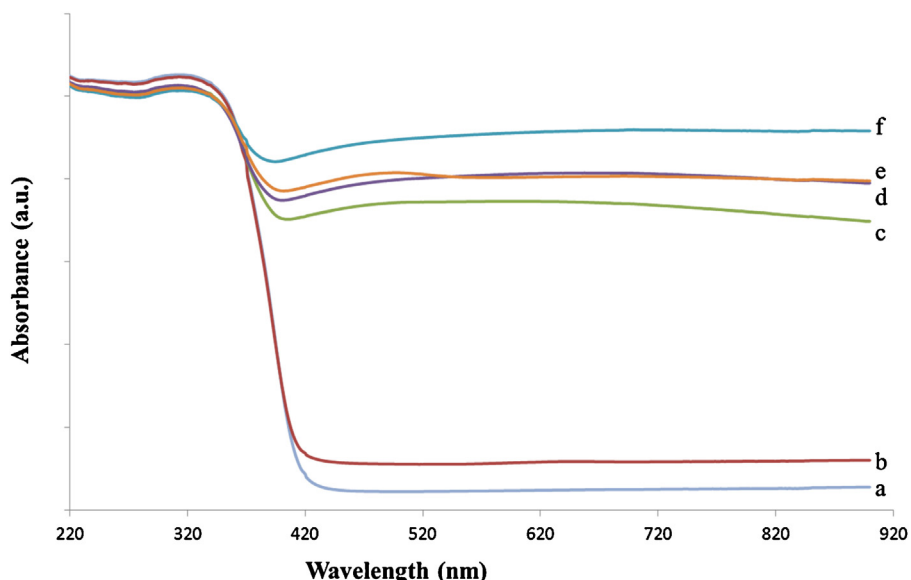


Fig. 5. UV-vis diffuse reflectance spectra of all tested photocatalysts: (a) P90, (b) P90/SPD, (c) 0.5%Pd/P90SPD, (d) 1%Pd/P90SPD, (e) 1%Pd/P90PD, (f) 2%Pd/P90SPD.

3.2. Photocatalyticactivity

Photocatalytic oxidation of methanol in gas phase was chosen as a test reaction to evaluate catalytic properties of all synthesized systems. Activities of the materials were estimated basing on the methanol oxidation and carbon dioxide production. First of all, two control experiments were applied: (1) upon UV illumination in the presence of pollutant in the air flow, without photocatalyst and (2) in the dark, in the presence of photocatalyst, pollutant in the air flow and at the temperature up to 100 °C (the results of these experiments are not presented here). In photolysis experiment neither methanol degradation nor CO₂ evolution was detected. In the second experiment, thermal test up to 100 °C, 1%Pd/P90/SPD photocatalyst was not active. Therefore, the conclusion is that this reaction depends on the presence of both light and photocatalyst.

Fig. 6 shows a progress of UV light driven photocatalytic oxidation of methanol in air in the presence of different titanium based systems. It is clearly seen that modification of TiO₂ with palladium using sonophotodeposition method resulted in a great enhancement of photocatalytic activity. Among this group 2%Pd/P90/SPD photocatalyst seems to be the most active material, as the complete degradation of methanol was achieved within the first 40 min of near-UV light illumination. A very high activity (>90% of degradation in 60 min) was also noted in the case of 1%Pd/P90/SPD photocatalyst and therefore this amount of Pd was chosen as an optimum. Three times lower activity was obtained for 1%Pd/P90/PD, the photocatalyst prepared by photodeposition method, showing a significant advantage of sonophotodeposition over photodeposition method in the preparation of materials with photocatalytic properties. This is a clear evidence of a great role of ultrasonication in the synthesis procedure. Similar activity values for bare TiO₂ photocatalysts and Pd photodeposited on TiO₂ material were noted in the following order: P90/SPD > P90 > 1%Pd/P90/PD (32% > 30% > 26% respectively). Herein, it is interesting a lower activity of photodeposited Pd sample in comparison with the bare TiO₂ material. Another observation arising interest is the profile curve of methanol degradation obtained for 0.5%Pd/P90/SPD photocatalyst. Initially, a very long activation is observed and then after ca. 100 min of illumination, an immediate increase of activity is clearly seen resulting in above 60% of methanol degradation reached in this case. All photocatalysts were stable during the whole time of illumination (180 min).

During photocatalytic reaction methanol undergoes oxidative decomposition through several organic intermediates from formaldehyde (HCHO), formic acid (HCOOH), carbon monoxide (CO), up to complete oxidation to CO₂ and H₂O [16]. The production and further decomposition of formaldehyde and slight amount of formic acid were observed in our conditions, following the mass signals during the reaction. Evolution of carbon dioxide, resulting from oxidation of methanol is shown in Fig. 7 in terms of selectivity as a function of illumination time. Among all tested materials the best selectivity results were obtained for Pd modified TiO₂ photocatalysts prepared by sonophotodeposition method. After 40 min of illumination selectivity to CO₂ reached 80% for both photocatalysts 2%Pd/P90/SPD and 1%Pd/P90/SPD, confirming a good selection of 1 wt.% of Pd as an optimum amount. In the shape of CO₂ selectivity curve, obtained for 0.5%Pd/P90/SPD photocatalyst, a rapid increase is observed after 80 min of illumination, like in the profile curve of methanol decomposition. The selectivity obtained by this material reached 50% after 100 min of illumination time. In comparison, in the case of 1% of Pd photodeposited on TiO₂ selectivity ca. 20% was reached. The values of turnover frequencies (TOF), calculated for photocatalysts containing 1 wt.% of palladium, were also compared (the amount of surface available Pd atoms was estimated from XPS data). It was found that TOF value increased from 4.9 mmol CO₂ mmol⁻¹ Pd s⁻¹ for 1%Pd/P90/PD to 43.2 mmol CO₂ mmol⁻¹ Pd s⁻¹ for 1%Pd/P90/SPD indicating almost 9 times more turnovers of methanol to CO₂ per second in the reaction with the photocatalyst prepared by sonophotodeposition method. It may be assumed that the conditions of sonophotodeposition process favour the formation of active Pd-TiO₂ hybrid species participating in the reaction and that metallic palladium deposited on TiO₂ is better catalyst in this reaction than PdO supported on TiO₂. Some interesting differences were noticed between bare TiO₂ photocatalysts. As in the methanol decomposition there was only a slight difference between those two systems, herein P90/SPD is more than two times better (selectivity to CO₂) than a commercial P90 (the obtained values are 25% and 10%, respectively). However, based on the results obtained from the characterization techniques used in this work, there were no significant differences in the physico-chemical properties of those materials and more investigations (e.g. electron spin resonance ESR) will help to understand the influence of ultrasonication and light on intrinsic properties of the material.

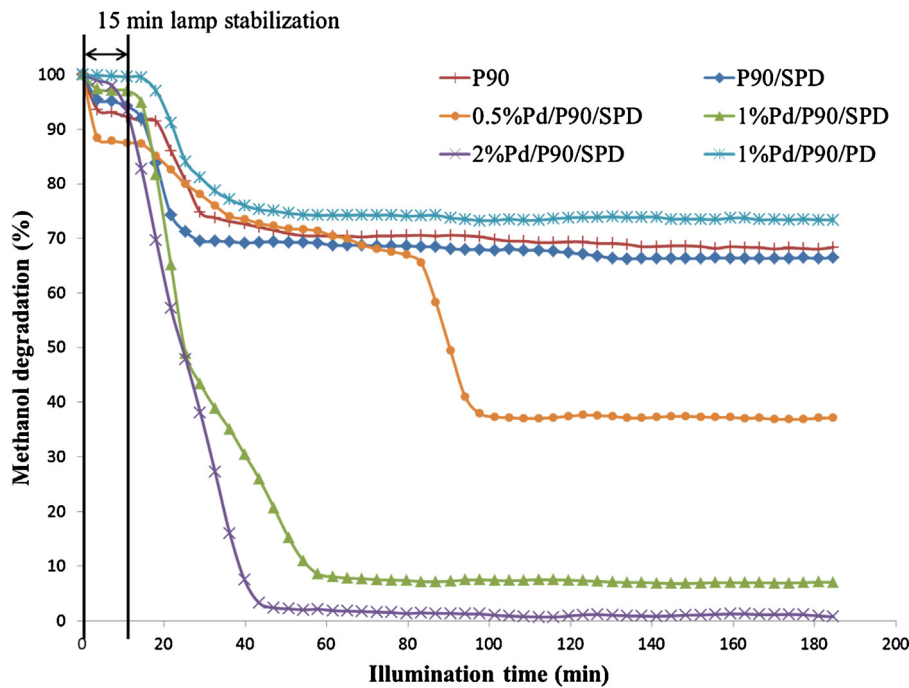


Fig. 6. Profiles of photocatalytic methanol degradation as a function of illumination time over palladium modified and bare TiO_2 materials.

The role of deposits of noble metals on semiconductor surfaces seems to be very well known. Many researchers claim that they act as efficient catalysts for electron transfer reactions. They also decrease the recombination probability of photoholes with their counterparts (electrons) and therefore increase the fraction of photoholes available for oxidizing interfacial charge-transfer reactions [44]. In air atmosphere, the electron trapped by Pd is transferred to O_2 and the superoxide anion is formed, $\text{O}_2^{\bullet-}$. After releasing the electron Pd can trap another one and the whole process repeats leaving the photohole free and capable to oxidize methanol. Superoxide itself is considered as poorly reactive as

it is not capable to react directly with chemical pollutants [45]. However, it can participate in total mineralization of organic compounds via reaction with organoperoxy radicals and production of H_2O_2 by $\text{O}_2^{\bullet-}$ disproportionation [46].

In the view of all investigation techniques described so far, the higher photocatalytic activity of Pd containing photocatalysts prepared by sonophotodeposition method should be related to a crystallite structure of deposited metal and the effects of ultrasonic irradiation. Metallic Pd was obtained by SPD method, whereas mainly PdO form was obtained by PD method, although in both procedures calcination in air flow at 300 °C for 4 h was the last

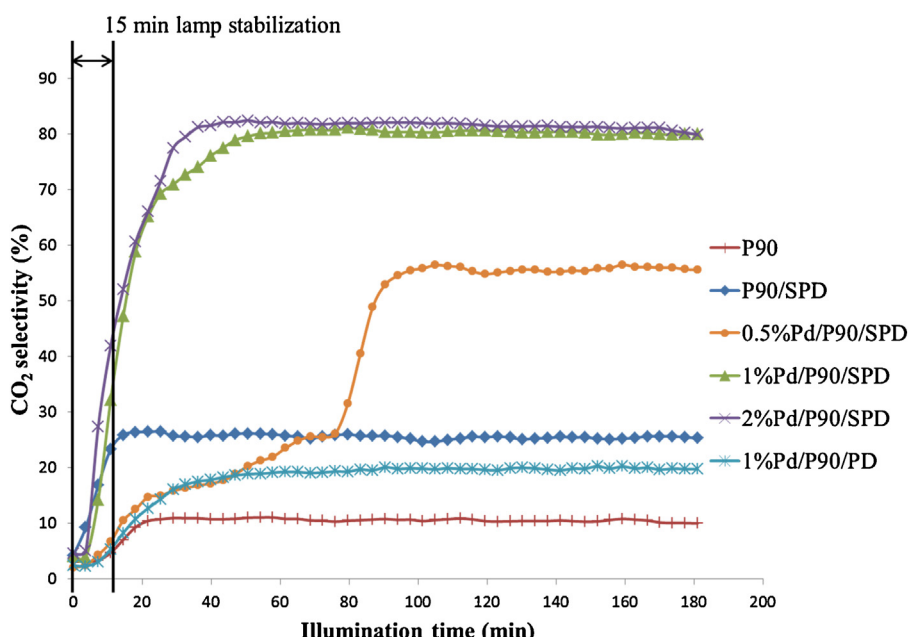
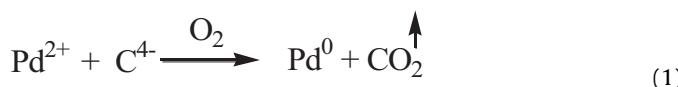


Fig. 7. Selectivity to carbon dioxide as a function of illumination time over palladium modified and bare TiO_2 materials.

step. It is supposed that the role of sonication is crucial in the synthesis and for the explanation of this phenomenon. Herein sonochemically generated radicals, like H^\bullet from sonolysis of water or some secondary radical species, are considered to act as reductants [25]. It is believed that these radicals can combine with oxygen atoms from the palladium (II) acetylacetone and therefore remove them from the organometallic precursor of palladium. At the same time, some part of metal ions can be reduced by these ultrasound-originated radicals and photo-electrons induced in the photodeposition process. Next, the material is subjected to calcination in air at 300 °C with the aim of removing the organic ligand of the palladium precursor. In the presence of carbon, remaining in the precursor, the oxygen from the air flow is consumed and palladium is reduced by the residual carbon following the reaction:



In contrast, during the photodeposition process, the excess of oxygen (this one remaining in the ligand precursor and in the air flow) oxidizes palladium to PdO form. The XPS results (Table 2) confirm that more oxygen remains in the matrix of photocatalyst prepared by photodeposition, ca. 60% of oxygen is bounded with carbon atoms in 1%Pd/P90/PD, whereas in the 1%Pd/P90/SPD photocatalyst the corresponding value is 7%. There is also more carbon left in 1%Pd/P90/PD (22.24%) than in 1%Pd/P90/SPD (12.53%) indicating that carbon is not so highly consumed in the redox process (Eq. (1)) during calcination in the case of photodeposition method.

In photocatalysis, the metallic form of palladium is better acceptor of electrons than the oxidized form (Pd^{2+}) therefore a lower recombination rate could be the reason of higher photocatalytic activity of the samples prepared by sonophotodeposition method.

4. Conclusions

A noble metal (e.g. palladium) can be deposited onto TiO_2 material (e.g. P90 Evonik) using so called sonophotodeposition method. Therefore, it was compared with known photocatalyst (commercial P90) and with additionally prepared Pd photodeposited TiO_2 in the photooxidation of methanol. Three different palladium loadings (0.5, 1, and 2 wt. %) were checked before the optimum was established on 1 wt. %. Sonophotodeposition, reported here for the first time, proved to be a successful tool in the synthesis of monometallic supported nanoparticles with photocatalytic properties. This method does not require the use of strong chemical reduction agent and is carried out in a short time, room temperature and atmospheric pressure. Although the 4 h calcination in air flow at 300 °C was the last synthesis step, several characterization techniques (e.g. XRD, XPS, TEM) confirmed that in the resulted photocatalysts palladium was in the metallic form. All materials prepared by sonophotodeposition method were active (>90%) in the photocatalytic decomposition of methanol in the gas phase and very selective to CO_2 (80% for 1% Pd containing sample).

Acknowledgements

This research was supported by a Marie Curie International Reintegration Grant within the 7th European Community Framework Programme. This scientific work was financed from the 2012–2014 Science Financial Resources, granted for the international co-financed project implementation (Project Nr. 473/7.PR/2012, Ministry of Science and Higher Education of Poland). This work was supported by the National

Science Centre (NCN) in Poland within research project DEC-2011/01/B/ST5/03888.

References

- [1] S. Wang, H.M. Ang, M.O. Tade, *Environment International* 33 (2007) 694–705.
- [2] Y.M. Kim, S. Harrad, R.M. Harrison, *Environmental Science & Technology* 35 (2001) 997–1004.
- [3] WHO guidelines for indoor air quality: selected pollutants, 2009, pp. 1–484 (in press).
- [4] R.M. Alberici, W.E. Jardim, *Applied Catalysis B: Environmental* 14 (1997) 55–68.
- [5] K. De Witte, V. Meynen, M. Mertens, O.I. Lebedev, G. Van Tendeloo, A. Sepulveda-Escribano, F. Rodriguez-Reinoso, E.F. Vansant, P. Cool, *Applied Catalysis B: Environmental* 84 (2008) 125–132.
- [6] W.K. Jo, K.H. Park, *Chemosphere* 57 (2004) 555–565.
- [7] M. Hussain, N. Russo, G. Saracca, *Chemical Engineering Journal* 166 (2011) 138–149.
- [8] J. Zhao, X. Yang, *Building and Environment* 38 (2003) 645–654.
- [9] H. Yu, K. Zhang, C. Rossi, *Journal of Photochemistry and Photobiology A: Chemistry* 188 (2007) 65–73.
- [10] L. Zou, Y. Luo, M. Hooper, E. Hu, *Chemical Engineering and Processing* 45 (2006) 959–964.
- [11] G.M. Zuo, Z.X. Cheng, H. Chen, G.W. Li, T. Miao, *Journal of Hazardous Materials B* 128 (2006) 158–163.
- [12] W.K. Jo, J.H. Park, H.D. Chun, *Journal of Photochemistry and Photobiology A: Chemistry* 148 (2002) 109–119.
- [13] F. Benoit-Marquie, U. Wilkenhoner, V. Simon, A.M. Braun, E. Oliveros, M.T. Mauvette, *Journal of Photochemistry and Photobiology A: Chemistry* 132 (2000) 225–232.
- [14] D.I. Kondarides, A. Patsoura, X.E. Verykios, *Journal of Advanced Oxidation Technology* 13 (2010) 116–123.
- [15] D.S. Bhatkhande, V.G. Pangarkar, A.A.C.M. Beenackers, *Journal of Chemical Technology and Biotechnology* 77 (2001) 102–116.
- [16] S.B. Sadale, K. Noda, K. Kobayashi, K. Matsushige, *Applied Surface Science* 257 (2011) 10300–10305.
- [17] J.C. Colmenares, R. Luque, J.M. Campelo, F. Colmenares, Z. Karpinski, A.A. Romero, *Materials* 2 (2009) 2228–2225.
- [18] M. Pelaez, N.T. Nolan, S.C. Pillai, M.K. Seery, P. Falaras, A.G. Kontos, P.S.M. Dunlop, J.W.J. Hamilton, J.A. Byrne, K. O’Shea, M.H. Entezari, D.D. Dionysiou, *Applied Catalysis B: Environmental* 125 (2012) 331–349.
- [19] M.C. Hidalgo, M. Maicu, J.A. Navio, G. Colon, *Journal of Physical Chemistry C* 113 (2009) 12840–12847.
- [20] S. Sakthivel, M.V. Shankar, M. Palanichamy, B. Arabindoo, D.W. Bahnemann, V. Murugesan, *Water Research* 38 (2004) 3001–3008.
- [21] V. Iliev, D. Tomova, R. Todorovska, D. Oliver, L. Petrov, D. Todorovsky, M. Uzunova-Bujanova, *Applied Catalysis A* 313 (2006) 115–121.
- [22] Y.Z. Yang, C.H. Chang, H. Idriss, *Applied Catalysis B* 67 (2006) 217–222.
- [23] O.T. Alaoui, A. Herissan, Ch.L. Quoc, M. el Mehdi Zekri, S. Sorgues, H. Remita, Ch. Colbeau-Justin, *Journal of Photochemistry and Photobiology A: Chemistry* 242 (2012) 34–43.
- [24] J.C. Colmenares, *Journal of Nanoscience and Nanotechnology* 13 (2013) 4787–4798.
- [25] J.H. Bang, K.S. Sulsick, *Advanced Materials* 22 (2010) 1039–1059.
- [26] J.C. Colmenares, A. Magdziarz, *Journal of Molecular Catalysis A: Chemical* 366 (2013) 156–162.
- [27] J.C. Colmenares, A. Magdziarz, K. Kurzydlowski, J. Grzonka, O. Chernyayeva, D. Lisovitskiy, *Applied Catalysis B: Environmental* 134–135 (2013) 136–144.
- [28] J.C. Colmenares, A. Magdziarz, O. Chernyayeva, D. Lisovitskiy, K. Kurzydlowski, J. Grzonka, *ChemCatChem* 5 (2013) 1–9.
- [29] Y. Han, J. Zhou, W. Wang, H. Wan, Z. Xu, S. Zheng, D. Zhu, *Applied Catalysis B: Environmental* 125 (2012) 172–179.
- [30] M.C. Hidalgo, J.J. Murcia, J.A. Navio, G. Colon, *Applied Catalysis A* 397 (2011) 112–120.
- [31] S.W. Lee, S. Obregon-Alfaro, V. Rodriguez-Gonzalez, *Journal of Photochemistry and Photobiology A: Chemistry* 221 (2011) 71–76.
- [32] L. Sun, J. Li, Ch. Wang, S. Li, Y. Lai, H. Chen, Ch. Lin, *Journal of Hazardous Materials* 171 (2009) 1045–1050.
- [33] J.C. Colmenares, A. Magdziarz, Polish Patent Application Number P. 401693, November 2012.
- [34] S. Sakthivel, H. Kisch, *Angewandte Chemie* 115 (2003) 5057–5060; S. Sakthivel, H. Kisch, *Angewandte Chemie International Edition* 42 (2003) 4908–4911.
- [35] R.A. Spurr, H. Myers, *Analytical Chemistry* 29 (1957) 760–762.
- [36] J.C. Colmenares, P. Lisowski, Polish patent application Nr P-405094, August 2013.
- [37] Y. Bi, G. Lu, *Applied Catalysis B: Environmental* 41 (2003) 279–286.
- [38] J.F. Moulder, W.F. Stickle, P.E. Sobol, K.D. Bomben, in: J. Chastain (Ed.), *Handbook of X-ray Photoelectron Spectroscopy*, Perkin-Elmer Corporation Physical Electronics Division, USA, 1992.
- [39] G. Ketteler, D.F. Ogletree, H. Bluhm, H. Liu, E.L.D. Hebenstreit, M. Salmeron, *Journal of the American Chemical Society* 127 (2005) 18269–18273.
- [40] M. Kruk, M. Jaroniec, *Chemistry of Materials* 13 (2001) 3169–3183.

- [41] S.J. Gregg, K.S.W. Sing, *Adsorption*, in: *Surface Area and Porosity*, Academic Press, London, 1982.
- [42] P. Weerachawanasak, P. Praserthdam, M. Arai, J. Panpranot, *Journal of Molecular Catalysis A: Chemical* 279 (2008) 133–139.
- [43] Z. Zhang, G. Mestl, H. Knozinger, W.M.H. Sachtler, *Applied Catalysis A* 89 (1992) 155–168.
- [44] A.A. Ismail, S.A. Al-Sayari, D.W. Bahnemann, *Catalysis Today* 209 (2013) 2–7.
- [45] P. Pichat, *Applied Catalysis B: Environmental* 99 (2010) 428–434.
- [46] Z. Wang, W. Ma, Ch. Chen, H. Ji, J. Zhao, *Chemical Engineering Journal* 170 (2011) 353–362.